RESEARCH PAPER

Effect of friction stir spot welding parameters on the microstructure and properties of joints between aluminium and copper

A. Habibizadeh[1] · M. Honarpisheh[1] · S. Golabi[1]

Abstract

The friction stir spot welding (FSSW) process of AA1050 and C10100 sheets using different process parameters was accomplished in two different configurations of Cu over Al (Cu-Al) and Al over Cu (Al-Cu). The experimental plan was designed according to response surface methodology (RSM), and the parameters were tool rotation speed, plunge depth and dwell time. Material flow, microstructure and microhardness of the optimum welded samples were examined using optical and scanning electron microscopy. The swirl mixing of materials, counter clockwise material flow and the streamlines of the plasticized metal were clearly observed at the stir zone (SZ) of the joints. For Al-Cu sheet configuration, the metals were not fully softened; therefore, plastic flow only occurred locally, which results in a small SZ. With the copper sheet on top, the size of the SZ enlarged. The Al-Cu configuration exhibited some lack of bonding at the sheet interface beneath the shoulder, and the copper ring extruded upward from the lower Cu plate into the upper Al plate with continuous intermetallic compounds (IMCs) developed at the interface. In the Cu-Al configuration, a discontinuous $CuAl_2$ layer developed at the interface of Al and Cu material with a $CuAl_2$ thickness of 160 μm. A $CuAl_2$–$CuAl$–Al_4Cu_9 laminated layer was developed at the hook interface. The hardness values were high in the SZ for all the produced spot samples; this was attributed to the presence of hard and brittle IMC compounds.

Keywords Friction stir spot welding · Optimization · Configuration · Failure mechanism · Microstructure · Microhardness

1 Introduction

Aluminium and copper alloy composite structures are ideal candidates to be used in chemical, nuclear, aerospace, transportation, power generation and electronics industries. Therefore, dissimilar joining of Al and Cu has attracted much attention and paved the way to the rapid development of dissimilar materials joining technology [1–6]. Producing sound Al–Cu dissimilar joints by fusion welding methods has always been a challenge for designers and engineers, due to their significant difference in chemical, physical and mechanical properties as well as high affinity to form brittle intermetallic compounds at high temperatures [7, 8]. Therefore, solid state joining processes such as

FSSW were extensively employed as an effective alternative for fusion welding processes [9].

The influence of the process parameters, i.e., tool rotation speed, plunge depth, tool design, dwell time and sheet configuration on Al/Cu weld strength, has been investigated by many researchers [10–20]. Mubiayi and Akinlabi [10] showed that the increasing shoulder plunge depth and tool rotational speed increase the maximum tensile failure load of the Al/Cu FSS welds. Investigating the fracture patterns showed that a nugget pull-out failure mode occurred in all the friction stir spot welds. Heideman et al.'s [11] findings show that the rotational speed of the tool has the most influence on the weld strength. In the microstructural evaluation of the welded joints, they observed that the strong welds have a copper ring extruded upwards from the lower copper sheet into the upper aluminium sheet, which helped increase interlocking and bonding between the two sheets. Also, the interface of the copper hook and the surrounding aluminium material was free from IMCs. While, they observed no clear copper ring in the weak joints, and a layered contiguous intermetallic structure tends to be formed along the interface which causes the shear strength of the welds to be less, compared to the joints with copper ring. Siddharth's

---

and Senthilkumar's [15] findings revealed that the lower plunge depth leads to insufficient frictional stir and weakens the joints' failure strength. Zhang et al. [21] stated that the Al/Cu FSSW joint tensile/shear strength is not affected significantly by dwell time. On the other hand, Kulekci [22] stated that the tensile shear strength of the joints was notably affected by the tool dwell time, with lower plunge depth, and tool speed. Li et al. [3] observed a Cu hook extruded upward from the lower Cu plate into the upper Al plate with intermetallic compounds (IMCs) developed on its interface in all joints. They stated that the dwell time has a direct effect on produced heat input during welding and IMC growth. At short dwell time, an intermittent $CuAl_2$ layer mixed with CuAl phase was observed at the joints' interface. However, continuous $CuAl_2$–CuAl–Al_4Cu_9 laminated layer developed at the interface at longer dwell time. Higher microhardness values were measured in the stir zone due to the presence of IMC particles and refined grains, compared to the other weld zones. Garg and Bhattacharya [13] studied the effect of various welding tool pin length and diameter on the shear strength of friction stir spot welded similar to Al-Al, Cu-Cu, and Cu-Al configurations. They stated that the formation of intermetallic compounds and their interlocking at the interface of sheets improves the resistance to crack propagation under the uniaxial tensile load. Mubiayi et al. [23] observed the copper particles and intermetallic compounds in the aluminium matrix of the welds formed during FSSW of aluminium and copper sheets.

A few investigations have been carried out on the FSSW of Al to Cu, but the basic issue of how the configuration of the metals would affect the joint strength remains untouched. Most of researchers have accomplished their studies with aluminium sheet as upper plate (Al-Cu configuration) due to the lower tool wear and weld peak temperature compared to Cu-Al configuration [24]. The work piece configuration effect documented is a bit contradictory. In FSW process of Al to Cu, Akbari et al. [4] found that when Al is placed on the top of Cu (Al-Cu arrangements), maximum fracture load of the joint is obtained. Aluminium alloy has lower thermal conductivity than copper alloy. When the welding tool shoulder is in contact with Al sheet (Al is placed on the top), a large amount of heat is generated in the weld area, which results in the formation of sound and fine grained zone in this area. On the other hand, as copper sheet has higher heat conductivity than Al sheet, when Cu is placed on top and tool shoulder is in contact with the copper plate, the

weld zone may not receive enough heat, which is needed for the sufficient plastic flow. Whereas, Regensburg et al. [6] mentioned that if the copper sheet is positioned on the top and is processed by the tool shoulder, intermixing of the sheets' material, as well as phase formation between the shear layers, improves significantly. Colmenero et al. [25] studied the optimization of Cu/Al FSSW parameters using response surface methodology (RSM). Garg and Bhattacharya [13] obtained higher shear strength for Cu-Al FSS welds compared to Al-Cu configuration.

However, the sheets' arrangement effect on the mechanical and metallurgical properties of the joints fabricated by FSSW process, has not been investigated systematically. In this paper, the effect of FSSW parameters, namely tool rotational speed, plunge depth and dwell time on shear failure load (SFL) of the Al-Cu and Cu-Al (different plate configuration) joints were investigated in a wider range, compared to the other published papers investigated. Optimum welding parameters for each configuration have been achieved using the results of design of experiments (DOE). Also, macroscopic characteristics, microstructure and microhardness of the welded samples that were fabricated in the optimum condition were investigated. There is no detailed study on the comparison of intermetallic compounds (IMCs) in the Al-Cu and Cu-Al configurations. Therefore, this work contributes to the understanding of the copper and aluminium sheets' configuration on the welded joints' properties.

2 Materials and methods

In the present work, two dissimilar sheet configurations were used. Aluminium (AA1050) and copper (C10100) sheets of thickness 2 mm and 100×40 mm dimensions with 40 mm overlap were used. The chemical compositions of the sheets are presented in Table 1.

A tool made of H13 steel (hardened to 52 HRC) with conical pin and concave shoulder (CCS profile), 2.5-mm pin length, 5-mm pin diameter and 14-mm shoulder diameter was employed. The sheets were tightly clamped in the fixture in lap configuration in the two configurations (Al over Cu and Cu over Al) in order to achieve the desired overlap (40 mm). The schematic of the welding setup, geometrical characteristics of the tool and the welding process setup with rotating tool and clamped sheets in the fixture is shown in Fig. 1. The spot overlap

Table 1 Chemical composition of the C10100 and AA1050 sheets

Material	Composition (wt. %)												
	Fe	Mg	Mn	Si	O	Zn	Pb	Co	B	Sb	Others	Cu	Al
AA1050	0.33	0.02	0.01	0.048	-	-	-	-	-	-	0.03	-	Bal
C10100	0.0008	-	-	-	0.0004	0.0002	< 0.003	-	-	0.0003	-	Bal	-

Fig. 1 (**a**) Dimension of lap shear tensile specimen (all dimensions are in mm), (**b**) schematic of the tool used in the FSSW process, (**c**) the friction stir spot welding process setup
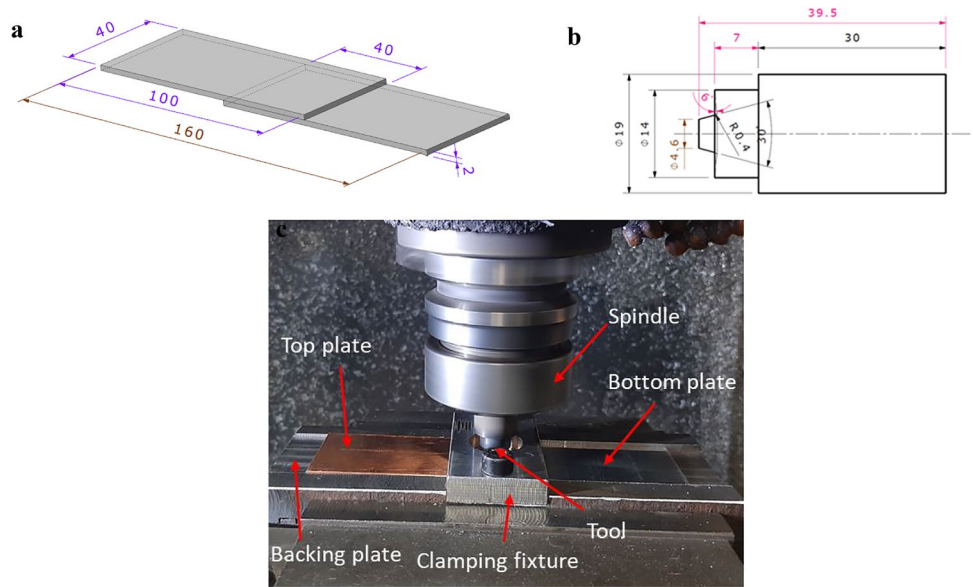
welds were produced using a CNC machine. The plunge rate of 10 mm/min was chosen for all experiments. Two cases regarding the position of Al with respect to Cu were considered. Dissimilar FSSW were carried keeping the upper sheet of copper and the lower sheet of AA1050 (hereafter donated as Cu-Al in the rest of the paper) and the upper sheet of AA1050 and the lower sheet of copper (hereafter donated as Al-Cu). Tensile shear testing of the welds was done using a "Koopa" universal testing machine with a crosshead speed of 1 mm/min.

In this work, the influence of tool rotation speed (R), dwell time (T) and tool plunge depth (D) on the shear strength of the joints produced by FSSW was investigated. A three-factor and five-level central composite design (CCD) consisting of 20 run sets for the Al-Cu configuration and 20 run sets for the Cu-Al configuration (totally 40 run sets) were used with the RSM to model the experimental layout. Table 2 shows the selected welding parameters and their suggested levels. A mathematical regression model describing the relationship between welding parameters and SFL was developed, and the optimal FSSW parameters are specified for each configuration using "Design-expert 11" software and confidence level of 95%. These models were analysed with analysis of variance (ANOVA) to identify the significant parameters. Table 3 shows the experimental plan details and the SFL.

After fitting a regression model for each configuration, the second set of experiments were performed to validate the regression models. Numerical optimization toolbox of "Design-Expert 11" software (desirability function) has been used to predict the optimal welding parameters that can produce the weld with the highest SFL. Several specimens produced at optimized welding condition were used for studying the model accuracy and further metallurgical analysis. Standard metallographic procedure was used for microstructure examination with nital2% reagent. Macroscopic cross-sections of the joints were observed by optical microscopy (OM). Microstructural observation was performed on a scanning electron microscope (SEM). Energy dispersive spectroscopy (EDS) analysis was performed for characterizing the intermetallic compounds and phases formed at the different welding zones. Vickers microhardness (HV) measurements were carried out in two lines on the cross-sections of the joints, along the centreline of the top sheet and the root of the bottom sheet with a 2.5-mm interval using 100 g load for 10 s (HV0.1).

3 Results and discussion

3.1 Developing an empirical equation

SFL of the welds strongly depends on welding parameters and sheet configuration, as shown in Table 3. The highest SFL of 6900 N (run no. 6) was obtained for Cu-Al configuration at

Table 2 Welding parameters and their levels for Al-Cu and Cu-Al configuration

Factor	Name	Minimum	Maximum	Coded low	Coded high	Mean	Std. dev
A	Tool rotational speed (R) (rpm)	500	2500	$-1 \leftrightarrow 1000$	$+1 \leftrightarrow 2000$	1500	458.83
B	Dwell time (T) (s)	0	8	$-1 \leftrightarrow 2$	$+1 \leftrightarrow 6$	4	1.84
C	Plunge depth (D) (mm)	2.10	3.70	$-1 \leftrightarrow 2.5$	$+1 \leftrightarrow 3.3$	2.9	0.3671

Table 3 CCD design matrix and experimental results

Std	Run	Factor 1 A: tool rotational speed	Factor 2 B: dwell time	Factor 3 C: plunge depth	Cu-Al SFL	Al-Cu SFL
		RPM	Sec	mm	kN	kN
3	1	1000	6	2.5	1.9	0.9
17	2	1500	4	2.9	6.53	3.18
15	3	1500	4	2.9	6.58	3.26
1	4	1000	2	2.5	2.3	1.1
19	5	1500	4	2.9	6.67	3.57
14	6	1500	4	3.7	6.8	3.93
7	7	1000	6	3.3	5.26	3.01
8	8	2000	6	3.3	6.9	4.08
5	9	1000	2	3.3	6.29	3.82
16	10	1500	4	2.9	6.7	3.64
4	11	2000	6	2.5	4.18	1.9
20	12	1500	4	2.9	6.51	3.51
10	13	2500	4	2.9	4.21	2.15
2	14	2000	2	2.5	4.1	1.96
9	15	500	4	2.9	1.2	0.5
18	16	1500	4	2.9	6.35	3.55
12	17	1500	8	2.9	6.16	3.58
13	18	1500	4	2.1	0.6	0.1
6	19	2000	2	3.3	6.08	3.65
11	20	1500	0	2.9	6.02	3.6

a tool rotation speed of 1500 rpm, dwell time of 4 s and tool plunge depth of 3.7 mm. Whereas, the lowest SFL of 600 N (run no. 18) is obtained with a tool rotational speed of 1500 rpm, dwell time of 4 s and plunge depth of 2.1 mm. For Al-Cu configuration, the highest SFL of 4080 N (run no. 8) was obtained at a tool rotational speed of 2000 rpm, dwell time of 6 s and tool plunge depth of 3.3 mm. Whereas, the lowest SFL obtained is 500 N for the run no. 15 with tool rotation speed of 500 rpm, 4-s dwell time and 2.9-mm tool plunge depth. Therefore, the SFL of fabricated welds is a function of welding parameters, as expressed in Table 2 and Eq. (1):

$$SFL = f(R, D, T) \tag{1}$$

Central composite design (CCD) was used for optimizing process variables and extracting a second-order model, since it requires the least number of experiments for modelling. The process parameters' optimization via CCD was performed in three main steps. First, the CCD method is used for designing the experimental layout, as shown in Table 3. Second, the value of coefficients of an extracted mathematical model (generally, a second order quadratic model for FSSW process) was estimated (as expressed in Eq. (2)). Third the model's response SFL of the welded samples in two configurations) was predicted, and the model's accuracy was tested [26].

$$Y = \beta_0 + \sum_{i=1}^{k} \beta_i x_i + \sum_{i=1}^{k} \sum_{j=1}^{k} \beta_{ij} x_i x_j + \sum_{i=1}^{k} \beta_{ii} x_{ii}^2 + \varepsilon \tag{2}$$

where:

Y is the response (here, Y is SFL of the welded samples); β_0 is the intercept; β_i, β_{ij}; and β_{ii} are coefficients of linear effect; double interactions, x_i, x_j, are the independent variables or factors and ε is error.

The values of the coefficients in Eq. (2) were calculated using the Design Expert Software for each configuration. The final central composite design obtained for SFL of the Cu-Al and Al-Cu weldments with significant terms was a quadratic function shown in Eqs. (3) and (4), respectively.

$$
\begin{aligned}
SFL(Cu - Al) = & -59.42139 + 0.016783R - 0.236349T + 32.57486D \\
& + 0.000291RT + 0.017187TD - 0.001656RD \\
& - 3.90136E - 06R2 - 0.032273 - T2 - 4.54119D2
\end{aligned} \tag{3}
$$

$$
\begin{aligned}
SFL(Al - Cu) = & +3.44 + 0.3787R - 0.0425T + 1.02D + 0.1725RT \\
& - 0.12RD - 0.015TD - 0.5356R2 \\
& + 0.0307T2 - 0.3631D^2
\end{aligned} \tag{4}
$$

where:

R is the rotational speed; T is dwell (welding) time; and D is plunge depth. Equations (3) and (4) reveal how each of the variables or their interaction influences the SFL.

3.2 ANOVA

For the Cu-Al model, analysis of variance (ANOVA) of friction stir spot welding SFL is given in Table 4. The F-value of 190.61 implies the significance of the model. The model F-value is the ratio of the mean square of any individual term to the mean square of the residual. For the Al-Cu configuration, ANOVA of quadratic model for predicting tensile shear force loading is shown in Table 5. The F-value of 73.67 implies the significance of the model. The model terms with P-value less than 0.0500 are significant (Tables 4 and 5). Accordingly, A, C, AB, AC, BC, A^2, B^2 and C^2 are significant for Cu-Al model terms. Meanwhile A, C, AB and A^2 are significant for the Al-Cu model terms. On the other hand, P-values greater than 0.1000 are not significant terms. The "F-value" of 4.79 and 1.55 implies not significant "lack of fit" value relative to pure error.

Residual sum of squares (R-Sq) and adjusted R-Sq were used for evaluating the fitness of the developed mathematical models (Table 6 for the Cu-Al and Table 7 for the Al-Cu configuration, respectively).

The adjusted R-squared considers the number of independent variables used for predicting the target variable. It is better to use adjusted R-squared when there are multiple variables in the regression model. For Cu-Al configuration, the calculated R-Sq and adjusted R-Sq were 0.9633 and 0.9890, respectively, indicating that the higher amount of variability (98.90% of the SFL data) is being explained by the developed empirical model (Eq. (3)). Also, for Al-Cu configuration, the calculated R-Sq and adjusted R-Sq were 0.9238 and 0.9718, respectively, indicating that the developed empirical relation is highly significant (97.18% of the SFL data could be described). In both

Table 4 ANOVA of quadratic model for predicting tensile shear force loading for the Cu-Al configuration

Source	Sum of squares	df	Mean square	F-value	P-value	
Model	79.01	9	8.78	190.61	<0.0001	Significant
A—Tool rotational speed	8.31	1	8.31	180.40	<0.0001	
B—Dwell time	0.00391	1	0.0039	0.0848	0.7768	
C—Plunge depth	37.36	1	37.36	811.23	<0.0001	
AB	0.6786	1	0.6786	14.73	0.0033	
AC	0.8778	1	0.8778	19.06	0.0014	
BC	0.0015	1	0.0015	0.0328	0.8598	
A^2	23.92	1	23.92	519.32	<0.0001	
B^2	0.4190	1	0.4190	9.10	0.0130	
C^2	13.27	1	13.27	288.20	<0.0001	
Residual	0.4606	10	0.0461			
Lack of fit	0.3810	5	0.0762	4.79	0.0553	not significant
Pure error	0.0795	5	0.0159			
Cor total	79.47	19				

Table 5 ANOVA of quadratic model for predicting tensile shear force loading for the Al-Cu configuration

Source	Sum of squares	df	Mean square	F-value	P-value	
Model	29.22	9	3.25	73.67	<0.0001	Significant
A—Tool rotational speed	2.30	1	2.30	52.08	<0.0001	
B—Dwell time	0.0289	1	0.0289	0.6558	0.4369	
C—Plunge depth	16.73	1	16.73	379.58	<0.0001	
AB	0.2380	1	0.2380	5.40	0.0425	
AC	0.1152	1	0.1152	2.61	0.1370	
BC	0.0018	1	0.0018	0.0408	0.8439	
A^2	7.21	1	7.21	163.65	<0.0001	
B^2	0.0237	1	0.0237	0.5371	0.4805	
C^2	3.31	1	3.31	75.21	<0.0001	
Residual	0.4407	10	0.0441			
Lack of fit	0.2676	5	0.0535	1.55	0.3221	Not significant
Pure error	0.1731	5	0.0346			
Cor total	29.66	19				

Table 6 R-Sq, adjusted R-Sq and R-Sq prediction for the Cu-Al developed model

Std. dev	0.2146	R2	0.9942
Mean	5.07	Adjusted R^2	0.9890
C.V.%	4.24	Predicted R^2	0.9633
		Adeq precision	41.7688

Table 7 R-Sq, adjusted R-Sq and R-Sq prediction for the Al-Cu developed model

Std. dev	0.2099	R2	0.9851
Mean	2.75	Adjusted R2	0.9718
C.V.%	7.64	Predicted R2	0.9238
		Adeq precision	27.5530

models, the predicted R^2 values are in reasonable agreement with the adjusted R^2.

3.3 Effect of FSSW parameters on the SFL

The effect of welding parameters and their interaction effects can be analysed using 3D response graph and contour plots, offered by the Design-Expert software. Figures 2 and 3 show the 3D response graph and contour plots of SFL for Cu-Al and Al-Cu configurations, respectively. In these 3D response graphs and contour plots, the plunge depth was kept constant (C = 2.5, 2.9 and 3.3 mm) and tool speed and dwell time parameters are two varying parameters (A vs. B). As stated before (Table 3) and clear from these figures, under similar welding conditions, the strength of the joint (SFL) in the Cu-Al configuration is always higher than the Al-Cu configuration. For both configurations (Cu-Al and Al-Cu) (Figs. 2 and 3), increasing the tool rotational speed and welding time (keeping the plunge depth constant) raises the heat input and enhances material flow which results in increasing SFL value to its maximum. The SFL value then decreases with further increase in tool rotational speed and welding time. This behaviour of SFL has been reported by other authors as the result of the "hook defect," increased generated heat (increased thermal exposure), which reduces the joint strength [27–31]. Figure 2a–f show that when tool plunge depth increased from 2.5 to 2.9 mm for Cu-Al, initially the maximum SFL has been increased to a certain value, and further increase in plunge depth keeps the maximum achievable SFL constant [32]. For the Al-Cu configuration, it can be seen from Fig. 3a–f that increasing plunge depth from 2.5 to 3.3 mm, constantly increases maximum SFL.

The effect of dwell time on weld strength has been discussed. Increasing welding time (keeping tool rotation and

plunge depth constant) slightly increases and then decreases the value of SFL for Cu-Al configuration (Fig. 2). Dwell time has a tremendous effect on heat conduction and material flow in order to achieve a stronger bond. At the beginning of the welding process (dwell time is low), less heat is produced. As dwell time increases, the material of the sheets will be mixed together; plasticization takes place and leads to improved material movement. However, excessive welding time increases thermal exposure, intense material mixing which reduces material flow stress and formation of brittle intermetallic compounds at the interface which reduces the joint's SFL [28].

However, the SFL of the Al-Cu welds (Fig. 3) is not affected significantly by welding time, as enough heat input can be achieved almost at the beginning of the FSS welding cycle (lower thermal coefficient of Al sheet compared to copper). Further increase of dwell time slightly reduces the tensile strength of the welds. Same results were reported by Zhang et al. [21]. They reported that the joint strength of Al during the FSSW process decreases by increasing rotational speed, while it is not affected significantly by dwell time.

3.4 Fracture mechanism of Al-Cu and Cu-Al configurations

Figure 4 shows the SFL versus elongation for the Al-Cu and the Cu-Al samples with maximum shear failure strength (Sample No. 6 for the Cu-Al and No. 8 for the Al-Cu). The Al-Cu configuration reaches lower values of the maximum load and shows more ductile failure behaviour, whereas the Cu-Al samples still show significant deformation before failure. Nugget pull out fracture within the aluminium base material can be observed in Fig. 4. The maximum SFL for Cu-Al samples reaches higher peak values than Al-Cu configuration. Fracture pattern of the Cu-Al samples exhibit interfacial failure with necking of the aluminium sheet. The higher maximum values are caused by the increased interface area as can be seen on the residual material adhesions on the copper side (Figs. 5 and 6).

3.5 Optimizing FSSW process parameters using desirability function and validation

The desirability function analysis (DFA) is one of the most frequently used multi-response optimization techniques in practice. The desirability lies between 0 and 1, and it represents the closeness of a response to its ideal value. Design Expert software seeks to maximize this function. The responses with desirability value of 1 are most desirable response values. There may be two or more maximums because of curvature in the response surfaces and their combination in the desirability function [33]. Figure 7a, b (for Cu-Al and Al-Cu configurations, respectively), demonstrate the desirability values of the numerical optimization procedure in which the criterion was set, "in range" for tool
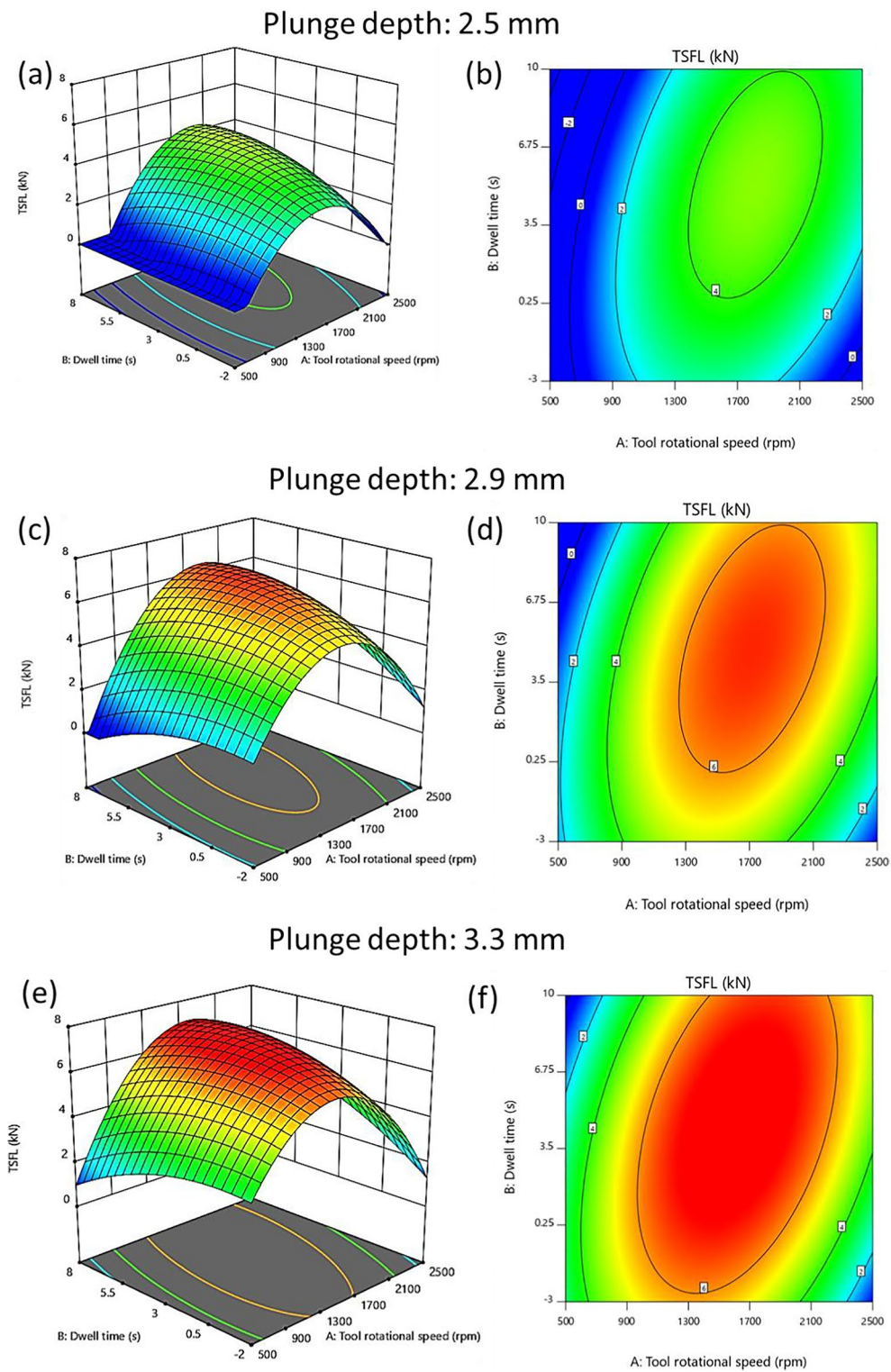
Fig. 2 R-T 3D response graph and contour plots at different plunge depths for the Cu-Al configuration

plunge depth, rotational speed and dwell time, and maximum SFL. The best maximum SFL was determined to be at tool rotational speed of 1318 rpm, dwell time of 3.1 s and plunge depth of 3.3 mm for Cu-Al configuration with the SFL value

of 7.16 kN and desirability of 1. Also, the best local maximum for Al-Cu configuration was found at tool rotational speed of 1600 rpm, dwell time of 3.16 s and plunge depth of 3.1 mm with the SFL of 4.14 kN.
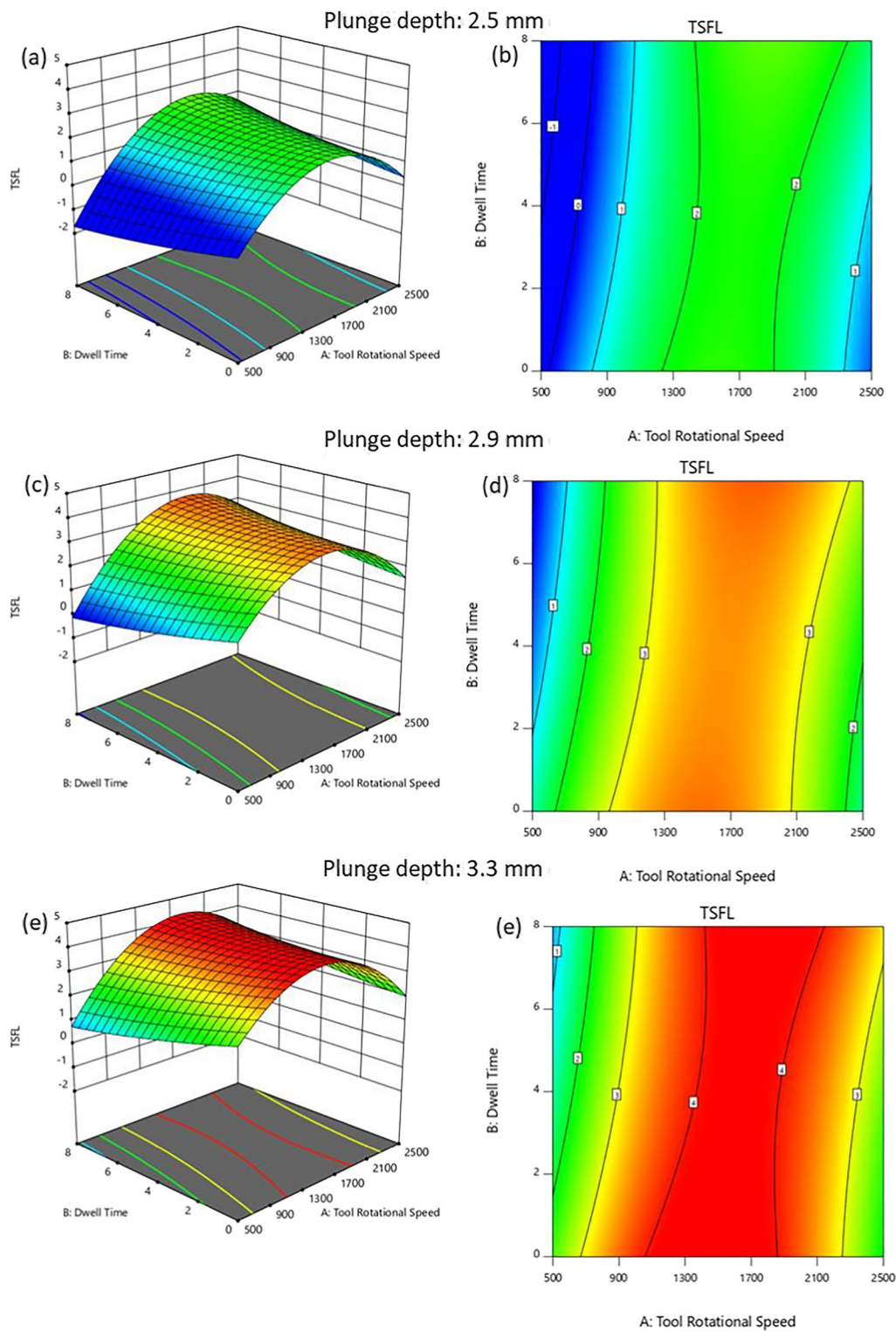
Fig. 3 R-T 3D response graph and contour plots at different plunge depths for the Al-Cu configuration

In order to validate the optimized parameters for each configuration, several welds were fabricated with the combination of welding parameters, as shown in Fig. 7. Three samples of dissimilar Al-Cu and Cu-Al FSSW joints were subjected to tensile test in the Tables 8 and 9. They represent a summary of process parameters, responses of accomplished tensile tests (according to Fig. 7) for Cu-Al and Al-Cu configurations, respectively. The results reveal that the optimal SFL
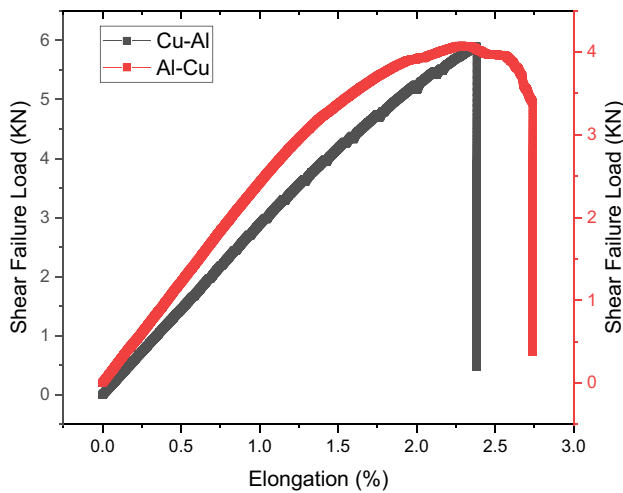
Fig. 4 Failure behaviour of the joints with maximum shear strength for (**a**) Al-Cu and (**b**) Cu-Al configurations

values were close to the results obtained from the mathematical model (offered by the DFA-optimal solution) for both configurations. The percentage of error between the optimal solution and the average validation test results for each configuration was obtained at 1.27 and 4.2% for Cu-Al and Al-Cu configurations, respectively. The value of the percentage error for each sheet configuration shows the accuracy of optimization procedure (< 5%) (Tables 8 and 9).

3.6 Macroscopic and microstructure evaluation of the welded joints

The first step to analyse the quality of the produced welds has to do with the control of macroscopic characteristics of the sheets after the welding process. The upper plate physical properties will influence the weld appearance and interface characteristics. When the Al plate is placed over the Cu plate, adequate material mixing flow took place due to the proper heat input which results in a good joint surface, as shown in Fig. 8a. When the sheet configuration was reversed and copper plate was place in top, as copper has higher melting point than aluminium, in order to have a proper plastic flow of the cu material, a high temperature is needed for good plastic flow of the Cu material. This higher temperature during Cu-Al welding led to the oxidation on the joint upper surface (Cu plate), as shown in Fig. 8b.

SEM (scanning electron microscopy) cross-sections of the welded samples at optimum condition (Fig. 7) for Al-Cu and Cu-Al configurations are shown in Fig. 9a, b. Four areas can be in the cross-section of the FSSW joints, namely stir zone (SZ) or dynamically recrystallized zone (DXY), thermo-mechanically affected zone (TMAZ), heat affected zone (HAZ) and base material (BM). SZ is located around the keyhole. Most of the
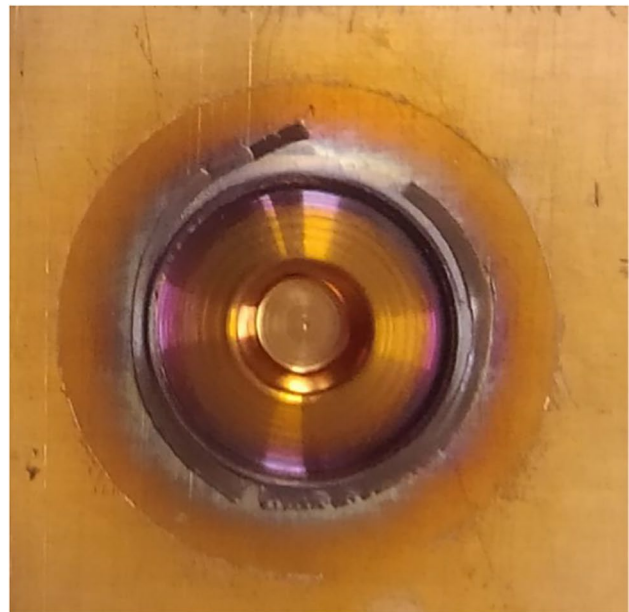

Fig. 5 View of the fractured surfaces for Cu-Al configuration with maximum shear strength

TMAZ area is on the bottom sheet. The area around SZ and TMAZ is HAZ. BM region is away from the weld. A detail of the SZ is demonstrated in Fig. 9c–f for both Cu-Al and Al-Cu configurations. The area near the key hole shows the stir zone (SZ) where both aluminium and copper sheets are well jointed due to high pressure and large plastic deformation during tool stirring and recrystallization, as shown in Fig. 9. e, f for both configurations. The height of the flash produced at the top surface of the upper plates, is smaller in Cu-Al configuration compared to Al-Cu. et al.-Cu specimens (Fig. 9a), softening of the

Fig. 6 View of the fractured surfaces for Al-Cu configuration with maximum shear strength

metals did not fully take place, and plastic flow only occurred in a small area, resulting in a small stir zone (SZ). With the copper sheet on top, the size of the SZ enlarged (Fig. 9b and f), which shows better material mixing in Cu-Al FSS-welded samples. Shen et al. [34] also reported the effect of SZ size on weld strength under shear load. The generated heat or degree of softening (in other words, the size of SZ) is related to physical property of the upper plate as tool shoulder deforms it. In the Al-Cu samples, a Cu hook (copper ring) was extruded upward from the lower Cu plate into the upper Al plate due to the extrusion and stirring exerted by the pin tool. While, in Cu-Al sheets position, copper was extruded downward from the upper Cu plate into the Al plate, which in both cases promote interlocking and bonding between the two sheets. Quantitative measurement analysis with "ImageJ" software shows the length of copper ring for Al-Cu configuration to be 0.988 mm, and the length of diffused copper from top to lower Al plate for Cu-Al sheet is 0.966 mm, which are approximately equivalent. The transition zone of the joints is distorted into a downward inclined interface, as shown in the TMAZ (Fig. 9a and b).

Due to the higher heat input, the increased softening of the metals allows Cu pieces to be separated from the Cu bulk and a layered structure, as shown in Fig. 9c formed through Al–Cu interaction. The Cu-Al sheet position increases the heat input due to plastic deformation [35]. The higher heat input in Cu-Al configuration allows intermetallic compounds to be formed at SZ (Fig. 9d). A qualitative visual inspection of the welds indicated the absence of apparent macroscopic defects for the Cu-Al configuration. Whereas, in the Al-Cu configuration some lack of bonding is observed at the interface. The incomplete bonding area is shown by the rectangular box in Fig. 9a. Two different zones namely "completely bonded zone" and "partially bonded zone" can be seen in Al-Cu welded samples. The fully bonded area is created by the rotating tool due to the severe plastic deformation, as can be seen in Fig. 9a. The presence of partially bonded region (Fig. 10) is consistent with the relatively low strength and ductility of the weld in tensile testing. According to findings of Firouzdor and Kou [36], the presence
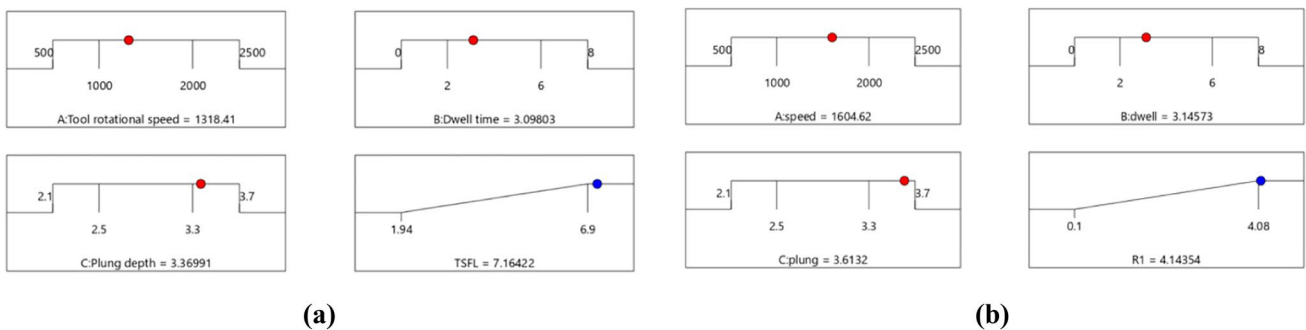

Fig. 7 Desirability ramp of SFL for (**a**) Cu-Al, (**b**) Al-Cu configuration

Table 8 Optimal parameters and confirmation test results for Cu-Al configuration

Experiment	Tool rotational speed (rpm)	Dwell time (s)	Plunge depth (mm)	SFL (kN)
Optimal solution of Cu-Al	1318	3.1	3.3	7.16
Run 1	1318	3.1	3.3	6.71
Run 2	1318	3.1	3.3	6.5
Run 3	1318	3.1	3.3	7.35
Average confirmation test results				7.07
Percentage error (%)				1.27

Table 9 Optimal parameters and confirmation test results for Al-Cu configuration

Experiment	Tool rotational speed (rpm)	Dwell time (s)	Plunge depth (mm)	SFL (kN)
Optimal solution of Cu-Al	1600	3.16	3.1	4.14
Run 1	1600	3.16	3.1	3.98
Run 2	1600	3.16	3.1	3.86
Run 3	1600	3.16	3.1	4.08
Average confirmation test results				3.97
Percentage error (%)				4.2

of partially bonded region leads to premature failure under the shearing action inherent during tensile testing of lap welds.

Tracing the material is a popular method for material flow pattern determination and has been employed by many researchers to trace material flow in FSSW joints [37, 38]. As the rotating tool penetrates into the lower sheet, the adhering layer of upper sheet material at the pin periphery is moved down and radially following the rotation of the welding tool. When the material beneath the tool pin is displaced upward, the weld keyhole forms. The top sheet material comes in contact with the tool shoulder; the material moves downward in the direction of the tool rotation. The plasticized material reaches the tip of the tool pin, and its flow direction is reversed due to the surrounding hard material. Then the material moves to the pin outside and upward to form a swirl path. The compressed material under the tool shoulder blocks the flowing material, and the material rotates along the pin and forms the flow morphology of the SZ [39]. For example, Fig. 9e shows the upward displacement of lower sheet material (copper) resulting from pin penetration. Microstructure in the Al-Cu configuration SZ in the vicinity of the interface is presented in Fig. 9e with the streamlines of the material indicated by the red arrow. Along the streamlines, IMC particles were dispersively distributed with some coarse particles showing a multiphase layered structure which is discussed later.

In Cu-Al FSSW process, the material of the lower plate (Al) is soft. When the tool moves downward, hard Cu material compresses the Al material below, causing concavity in the lower Al plate in the joint (Fig. 11a) [40]. It can be seen in Fig. 11a and b, for Cu-Al configuration, intense swirl mixing of materials

Fig. 8 Appearances of Al-Cu FSSW joints with configuration of: (**a**) Al on the top and Cu on the bottom; (**b**) Cu on the top and Al on the bottom
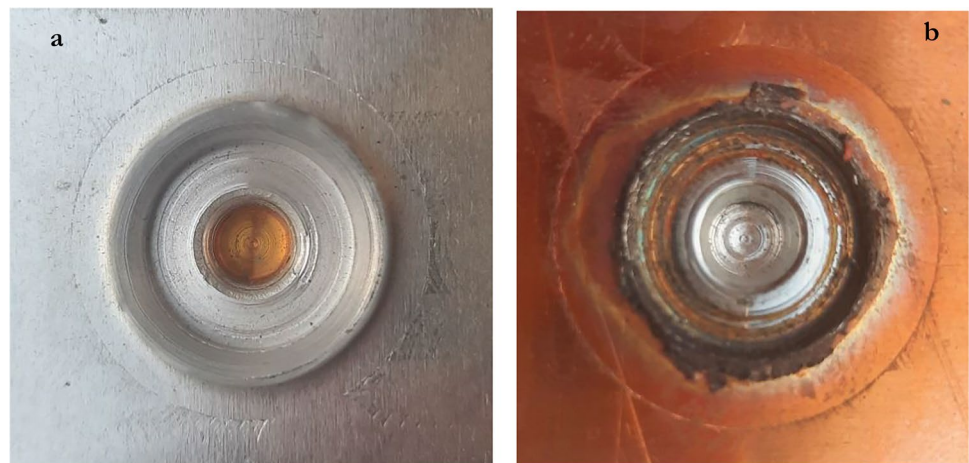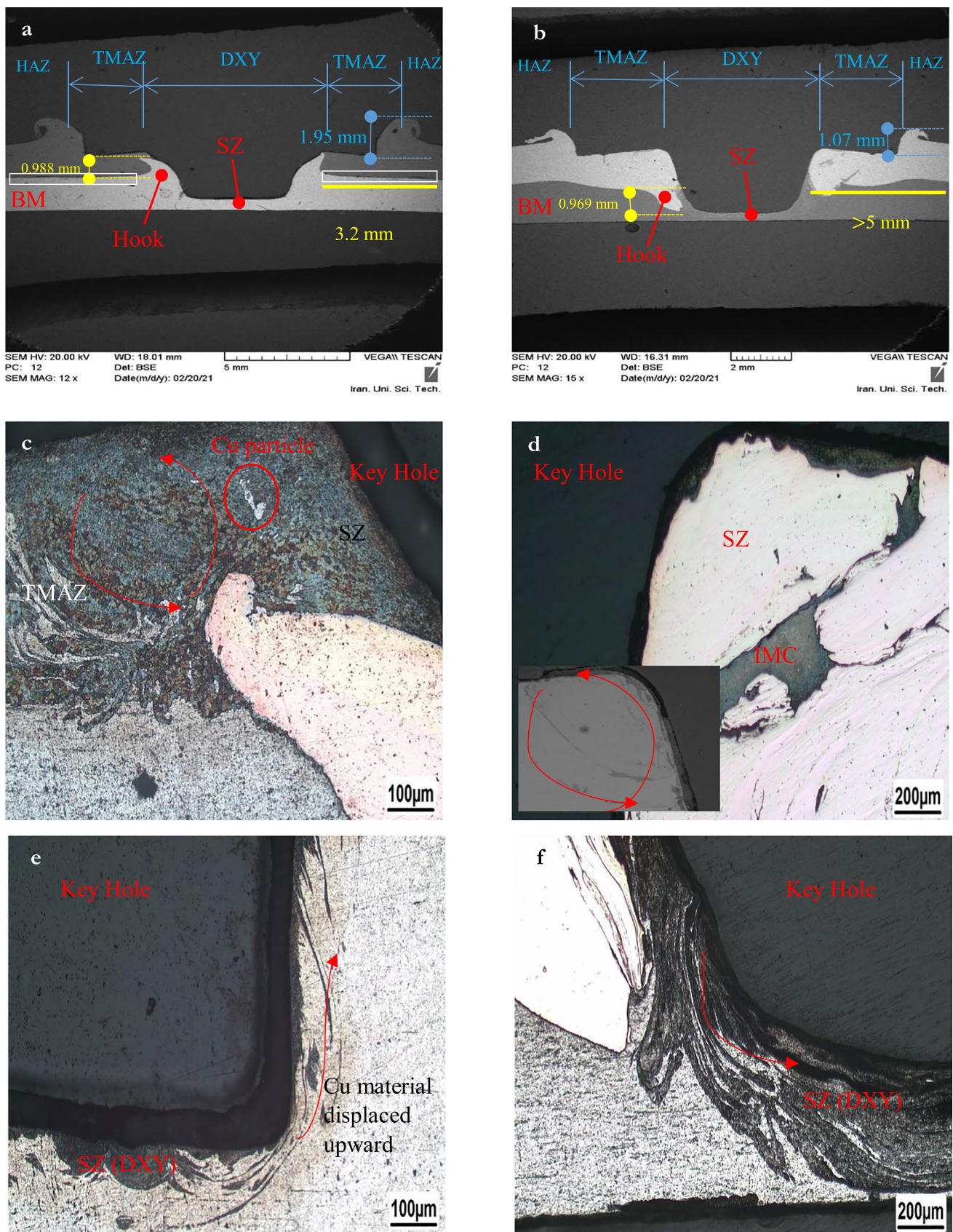
Fig. 9 Cross-section morphologies of the joints, different welding zones, (**a**) Al-Cu (**b**) Cu-Al (**c**) SZ (Al-Cu), (**d**) SZ (Cu-Al), (**e**) SZ (Al-Cu), (**f**) SZ (Cu-Al)
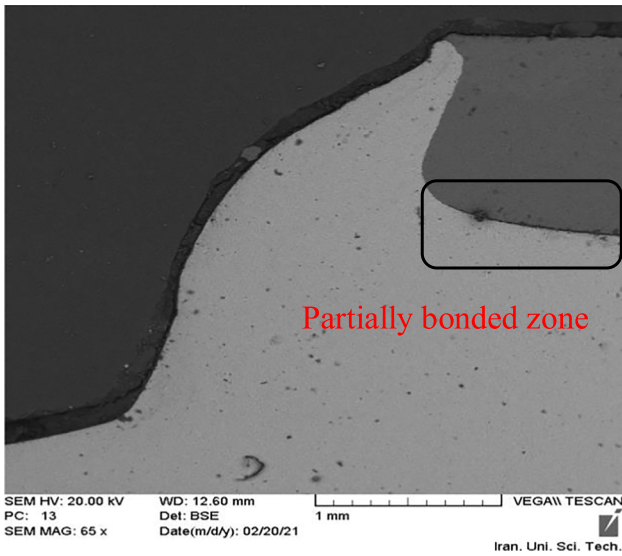
Fig. 10 Partially bonded zone in Al-Cu configuration

around the key hole occurred. A good material mixing, a distribution of copper particles and fragments with irregular shapes and different sizes, was observed in the aluminium matrix.

3.7 Interfacial microstructure evaluation

IMC formation at the interface of Al and Cu in the FSSW process is unavoidable. During FSSW, different Al-Cu IMCs are formed because of the heat input and flow of the base materials while subject to high forces. Because the chemical reactions that occur under the thermal cycles of the FSSW process are not close to the equilibrium condition, the formation of IMC at the joint interface is non-uniform and can be quite rapid. Furthermore, during the forming process of IMC, a small amount of formed IMC would be stripped off and dispersed in the matrix resulting from the stirring during FSSW, forming a discontinuous mixed pattern of the IMC layer. SEM images for the hook interface facing surrounding

Fig. 11 (a) Cup pattern in Cu-Al configuration, (b) downward movement of copper material
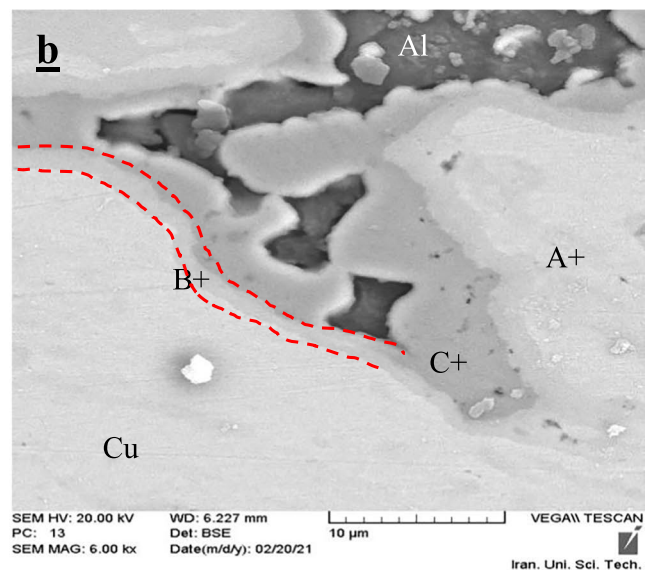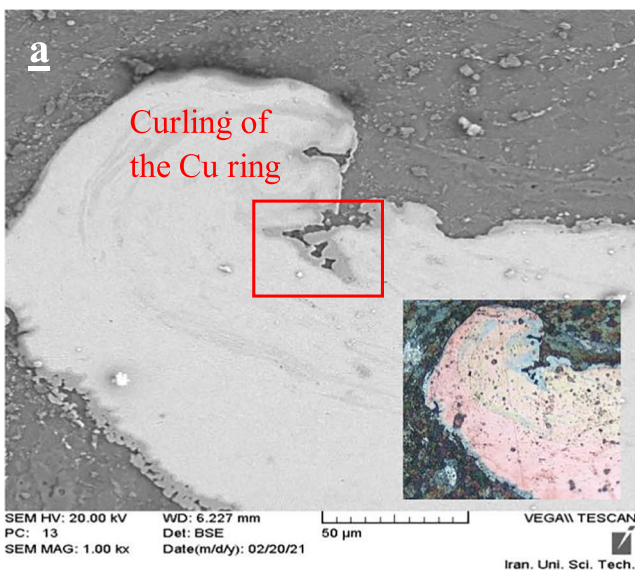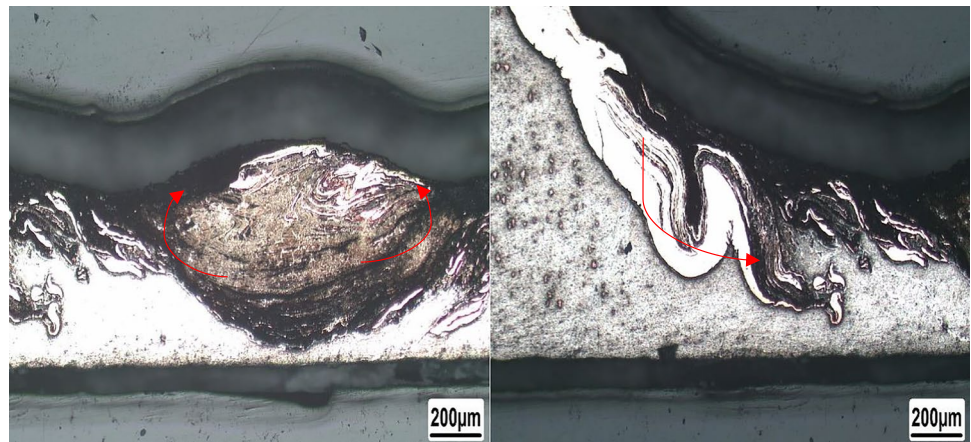

Fig. 12 (a) SEM microstructure of Hook/ SZ of Al-Cu configuration, (b) magnified view of the rectangular box shown in the left and EDS locations

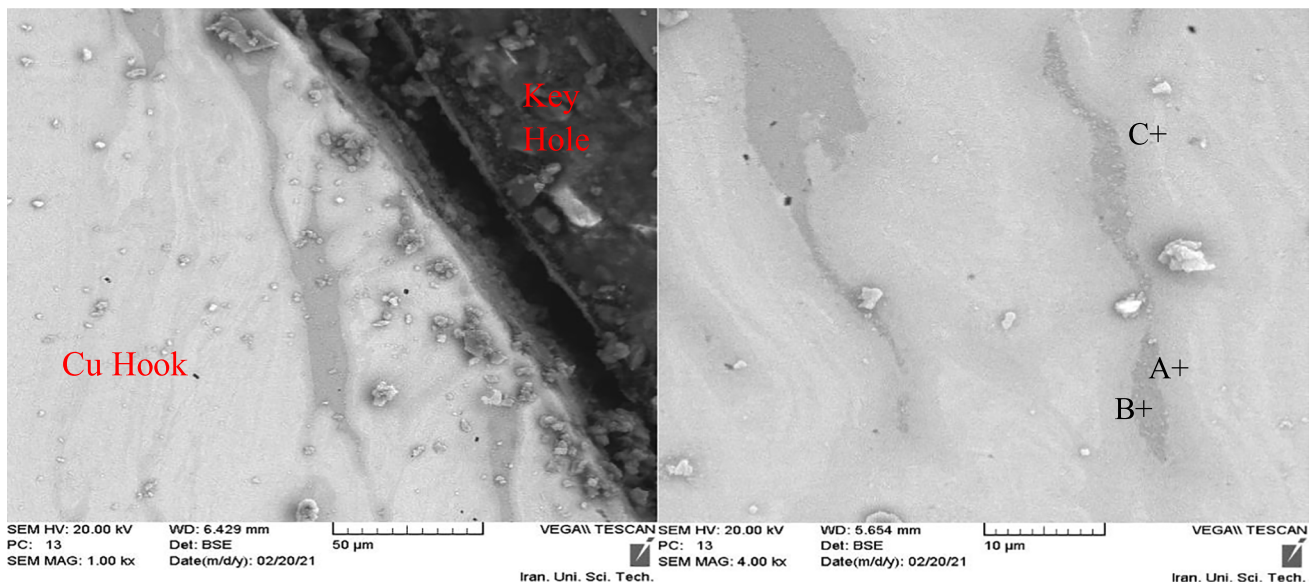**Table 10** EDS results of hook/SZ et al.-Cu configuration

Location of the ESD analysis	Element content (at.%)		Composition
	Al	Cu	
A	22.44	77.56	Al4Cu9
B	66.63	33.37	CuAl2
C	83.57	16.43	(Al) + CuAl2

Al matrix SZ et al.-Cu configuration are shown in Fig. 12a and b with the corresponding EDS results listed in Table 10. The copper ring extruded upward from the lower Cu plate into the upper Al plate with continuous intermetallic compounds (IMCs) developed on its interface. A magnified image of the left side hook of the Al-Cu weldments is shown in Fig. 12b. A continuous $CuAl_2$–$CuAl$–Al_4Cu_9 laminated layer developed at the whole hook/SZ interface. Heat input in Al-Cu FSS-welded samples accelerates the growth of IMC at the Al-Cu interface due to the thermal-activated

nature of IMC. An Al_2Cu layer with a thickness of 1.2 μm was shown by red dash lines.

On the Al-Cu hook interface back at the keyhole in the joint, a discontinuous Al_2Cu-$AlCu$-Al_4Cu_9 layer was observed at the optimum welding condition. The EDS analysis of IMCs stripped off and formed in the interface, as shown in Fig. 13 and Table 11.

In Cu-Al configuration, an intermittent $CuAl_2$ layer developed at the part of the interface of Al and Cu material with the thickness of 160 μm which was shown by red dash lines (Fig. 14), resulting from the high heat input. Due to the heat input at the optimum condition, $CuAl_2$–$CuAl$–Al_4Cu_9 (Table 12) laminated layer was developed at the part of the hook interface, as shown in Fig. 14. The presence of intermetallic compounds with high thickness can reduce the ductility of the joint and increase the resistance to crack growth. However, the absence of intermetallic compounds in the part of the welded joint improves the ductility and increases the weld strength considerably [13]. The EDS analysis of IMCs stripped off and dispersed in the matrix, is shown in Fig. 15 and Table 13.

Fig. 13 (**a**) SEM microstructure of hook back at the keyhole of Al-Cu configuration, (**b**) EDS locations

Table 11 EDS results of IMC'S at Cu matrix (Al-Cu)

Location of the ESD analysis	Element content (at.%)		Composition
	Al	Cu	
A +	67.52	32.48	CuAl2
B +	82.86	17.14	(CuAl) + CuAl2
C +	38.95	61.05	Al4Cu9

Table 12 EDS results of hook/SZ at Cu-Al configuration

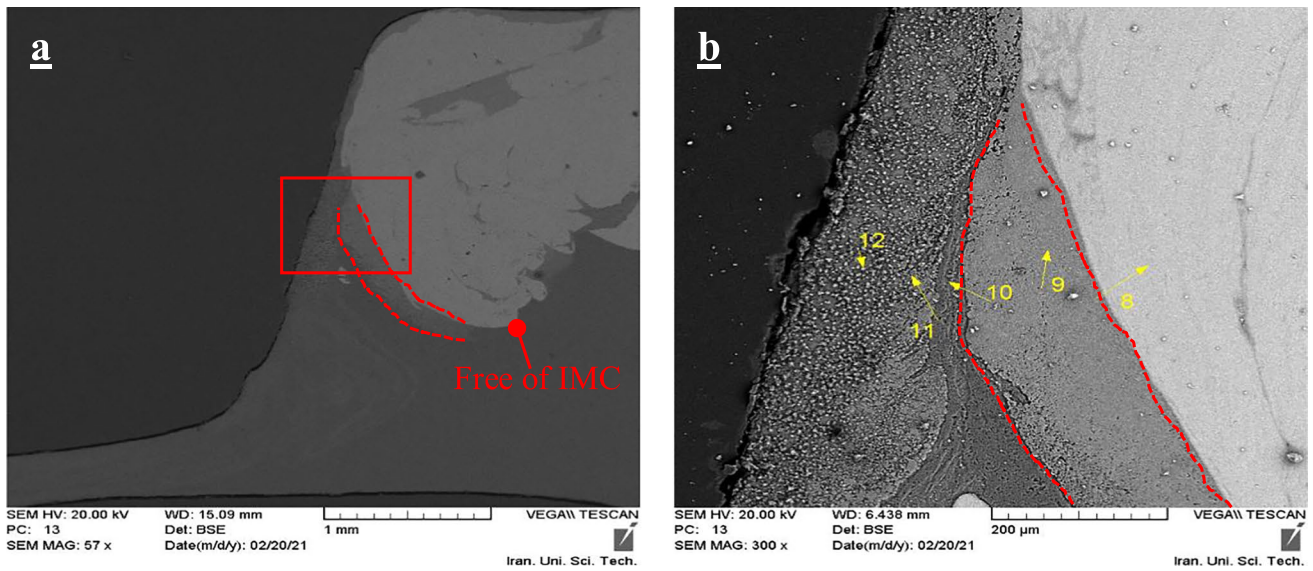| Location of the ESD analysis	Element content (at.%)		Composition
	Al	Cu	
8	22.26	77.74	Al4Cu9 + Cu
9	80.69	19.31	CuAl2
10	98.40	1.60	Al
11	83.97	16.03	(CuAl) + CuAl2
12	54.89	45.11	CuAl

Fig. 14 SEM microstructure of Cu-Al configuration Interface, (**b**) magnified view of the rectangular box shown in the left and EDS locations

Table 13 EDS results of IMCs et al. matrix (Cu-Al)

Location of the ESD analysis	Element content (at.%)		Composition
	Al	Cu	
A +	62.53	37.47	CuAl2
B +	28.52	71.48	Al4Cu9

3.8 Comparison of Al-Cu and Cu-Al configurations

Differences in the Cu-Al and Al-Cu configurations are summarized in Table 14. Due to the lower heat transfer coefficient of Cu compare to Al, the Cu-Al configuration experiences higher heat input than Al-Cu configuration. Higher heat input leads to a larger stir zone (SZ) and better material mixing in the Cu-Al configuration. Poor material mixing in the Al-Cu configuration (metals were not fully softened) leaves a partially bonded zone which limits the
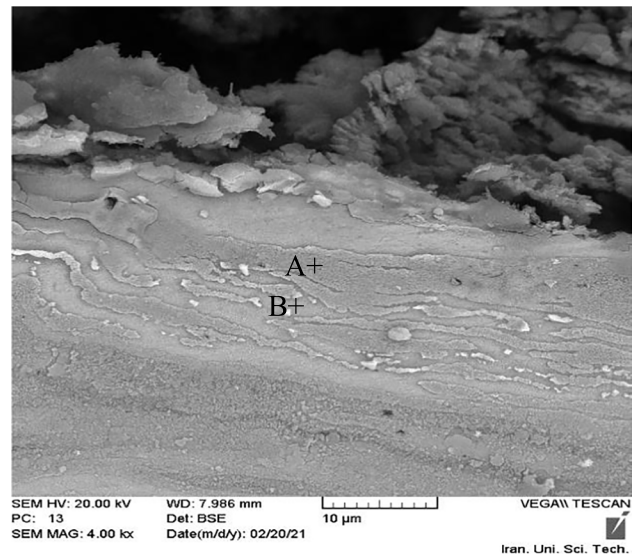

Fig. 15 SEM microstructure of hook back at the keyhole of Cu-Al configuration, (**b**) EDS locations

Table 14 Differences of Al-Cu and Cu-Al configurations

Configuration	IMCs			Macro inspection	SZ size	Heat input
	SZ/hook interface	Thickness	Hook/key hole interface			
Al-Cu	Continuous CuAl2–CuAl–Al4Cu9	1.2 μm CuAl2-continuous	Discontinuous Al2Cu–AlCu–Al4Cu9	Partially bonded zone	Smaller than Cu-Al	Lower than Cu-Al
Cu-Al	Discontinuous CuAl2–CuAl–Al4Cu9	160 μm CuAl2-discontinuous	Laminated Al2Cu–Al4Cu9	Fully bonded zone	Larger than Al-Cu	Higher than Al-Cu

Fig. 16 Photographs of the failed (**a**) Cu-Al and (**b**) Al-Cu specimens, welded at optimum condition

shear strength, compared to the Cu-Al configuration. The high heat input in the Cu-Al configuration leads to the formation of a thicker IMC layer than the Al-Cu configuration, increases the resistance to crack growth and reduces
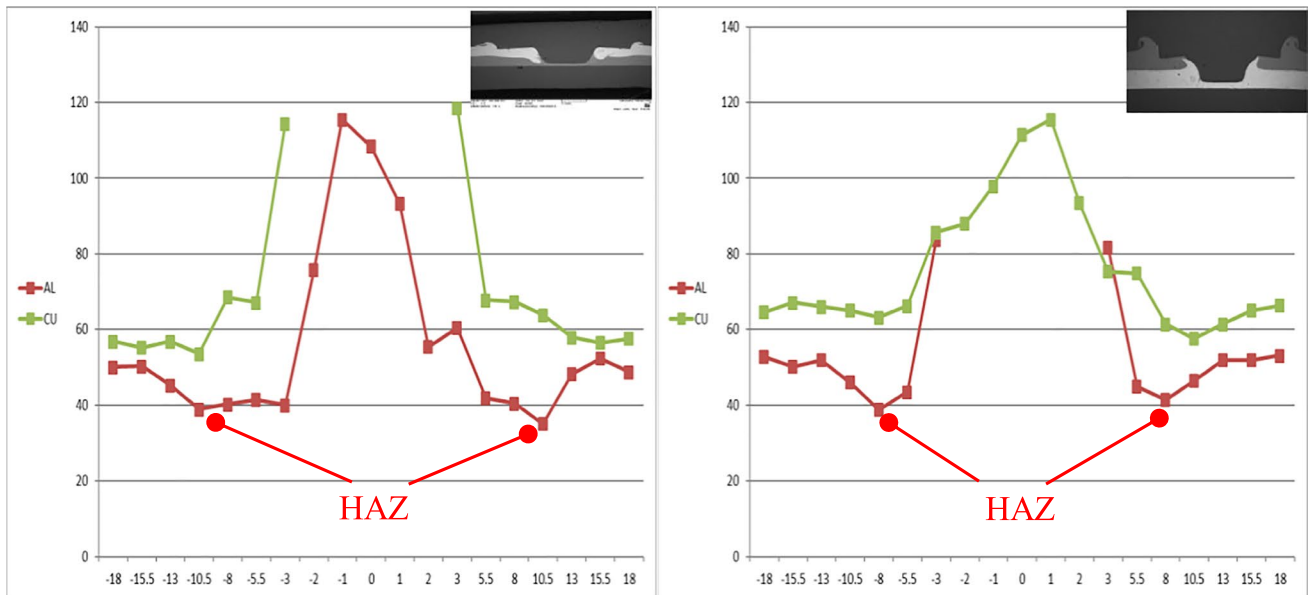

Fig. 17 Microhardness profiles of the joints for (**a**) Cu-Al and (**b**) Al-Cu configurations

ductility. However, since the IMCs of the copper–aluminium configuration at the interface of the stir zone/hook and hook/key hole are intermittent, these joints have sufficient ductility for industrial applications.

3.9 Fracture mechanism of Al/Cu spot welded at optimum condition

Figure 16 shows the different types of fracture patterns of the joints under lap shear loading. Nugget pullout failure pattern was observed for both Al-Cu and Cu-Al joints.

The crack moves from the tip of the hook in the direction of the weld area and the nugget separates from the top plate, leaving a circular hole in the top plate. Badarinarayan et al. [41] reported that the hook formation determines the weld strength of the joint. With the formation of the hook, a large amount of strain accumulates in the weld area at the bottom of the tool shoulder (tool shoulder corner), and also the thickness of the upper sheet is significantly reduced. Therefore, hook formation and high strain localization lead to reduced strength of the weld. As a result, the crack spreads from the hook tip to the top plate in the direction of the welding periphery, which eventually leads to the separation of the two sheets from the circumference (shown in Fig. 16a,b).

3.10 Microhardness

Figure 17 shows the hardness profiles of the joints for Al-Cu and Cu-Al configurations. Due to the weld keyhole, the hardness profile on the top sheet is discontinuous. In a typical Al-Cu and Cu-Al FSSW joint, the Al sheet is softer than the Cu sheet material in the BM regions, while in the Hook area, microhardness values increase significantly due to the presence of copper in the aluminium matrix. The values of microhardness in the SZ near the keyhole show a sudden increase due to the presence of hard and brittle intermetallic compounds (Figs. 13 and 15).

In the Cu-Al FSSW, the hardness distribution of the joint is slightly different from that of the Al-Cu FSSW. In both configurations, the hardness in the HAZ of the bottom Al and copper sheet is lower than that of the Al BM; this is due to the coarsening of the grain resulting from the heating of the material.

4 Conclusion

In this paper, AA1050 aluminium alloy was successfully welded to Cu sheet using the FSSW method. The following important results were obtained.

Mathematical models describing the relationship between welding parameters and SFL are developed and the optimal FSSW parameters are specified for each configuration using "Design Expert" software with less than 4.2% discrepancy. The

maximum SFL of 7.16 kN and 4.14 kN were obtained for the Cu-Al and Al-Cu configurations, respectively at the optimal condition.

Circulating flow "swirl" pattern and counter clockwise material flow and the streamlines of the plasticized metal were observed in the FSSW process. Due to the lower heat transfer coefficient of Cu compared to Al, the Cu-Al configuration experiences higher heat input than Al-Cu configuration. Higher heat input leads to a larger stir zone (SZ) and better material mixing in the Cu-Al configuration. Poor material mixing in the Al-Cu configuration (metals were not fully softened) leaves a partially bonded zone which limits the shear strength compared to the Cu-Al configuration. The high heat input in the Cu-Al configuration leads to the formation of a thicker IMC layer (160 μm) than the Al-Cu configuration (1.2 μm) and reduces ductility. However, since the IMCs of the copper–aluminium configuration at the interface of the stir zone/hook and hook/key hole are intermittent, these joints have sufficient ductility for industrial applications. Both the Al-Cu and Cu-Al configurations fail under plug-type fracture mode.

Declarations

References

1. Zhang W, Shen Y, Yan Y, Guo R, Guan W, Guo G (2018) Microstructure characterization and mechanical behavior of dissimilar friction stir welded Al/Cu couple with different joint configurations. Int J Adv Manuf Technol 94(1):1021–1030

2. Zhang C, Shirzadi AA (2018) Measurement of residual stresses in dissimilar friction stir-welded aluminium and copper plates using the contour method. Sci Technol Weld Joining 23(5):394–399

3. Li, Gaohui, et al. Influence of dwell time on microstructure evolution and mechanical properties of dissimilar friction stir spot welded aluminum–copper metals. J Mater Res Technol 8.3 (2019): 2613–2624.

4. Akbari M, Abdi Behnagh R, Dadvand A (2012) Effect of materials position on friction stir lap welding of Al to Cu. Sci Technol Weld Joining 17(7):581–588

5. Li M, Zhang C, Wang D, Zhou L, Wellmann D, Tian Y (2020) Friction stir spot welding of aluminum and copper: a review. In: Materials 13, No. 1, 156. Switzerland. 1996–1944

6. Regensburg A, Petzoldt F, Benss T, Bergmann JP (2019) Liquid interlayer formation during friction stir spot welding of aluminum/copper. Welding World 63(1):117–125

7. Pérez M, Parte D, Azofra JC, Domingo H, Fals C, Roca AS, César M, Orozco S, Macías EJ (2019) A new way to predict the mechanical properties of friction stir spot welding for Al-Cu joints by energy analysis of the vibration signals https://doi.org/10.1007/s00170-019-04396-5

8. Siddharth S, Senthilkumar T, Chandrasekar M (2017) Development of processing windows for friction stir spot welding of aluminium Al5052 /copper C27200 dissimilar materials. Trans Nonferrous Met Soc China (English Ed. 27 (2017) 1273–1284. https://doi.org/10.1016/S1003-6326(17)60148-1.

9. Mubiayi MP, Akinlabi ET, Makhatha ME (2019) Current trends in friction stir welding (FSW) and friction stir spot welding (FSSW) https://doi.org/10.1007/978-3-319-92750-3.

10. Mubiayi MP, Akinlabi ET (2016) Evolving properties of friction stir spot welds between AA1060 and commercially pure copper C11000. Trans Nonferrous Met Soc China (English Ed. 26 1852–1862. https://doi.org/10.1016/S1003-6326(16)64296-6

11. Heideman R, Johnson C, Kou S (2010) Metallurgical analysis of Al/Cu friction stir spot welding. Sci Technol Weld Join 15:597–604. https://doi.org/10.1179/136217110X12785889549985

12. Shiraly M, Shamanian M, Toroghinejad MR, Jazani MA, Sadreddini S (2017) The influence of tool geometry on the mechanical behaviour of FSSWed Al/Cu ARBed Composite. Trans Indian Inst Met 70:2205–2211. https://doi.org/10.1007/s12666-017-1044-7

13. Garg A, Bhattacharya A (2017) Strength and failure analysis of similar and dissimilar friction stir spot welds: influence of different tools and pin geometries. Mater Des 127:272–286. https://doi.org/10.1016/j.matdes.2017.04.084

14. Siddharth S, Senthilkumar T (2018) Optimizing process parameters for increasing corrosion resistance of friction stir spot welded dissimilar Al-5086/C10100 joints. Trans Indian Inst Met 71:1011–1024. https://doi.org/10.1007/s12666-017-1236-1

15. Siddharth S, Senthilkumar T (2017) Study of tool penetration behavior in dissimilar Al5083 /C10100 friction stir spot welds. Procedia Eng 173:1439–1446. https://doi.org/10.1016/j.proeng.2016.12.209

16. Sun H, Zhou Q, Zhu J, Peng Y (2017) Analysis on the fracture of Al-Cu dissimilar materials friction stir welding lap joint. J Mater Eng Perform 26:5715–5722. https://doi.org/10.1007/s11665-017-3029-4

17. Abbass MK, Hussein SK, AAK (2015) Optimization of friction stir spot welding parameters of dissimilar welded joints of aluminum alloy (AA2024T3) with pure copper sheets. Int J Eng Sci Res Technol 9655 514–526.

18. Manickam S, Balasubramanian V (2015) Maximizing strength of friction stir spot welded bimetallic joints of AA6061 aluminum alloy and copper alloy by response surface. 3 15–26.

19. Shiraly M, Shamanian M, Toroghinejad MR, Ahmadi Jazani M (2014) Effect of tool rotation rate on microstructure and mechanical behavior of friction stir spot-welded Al/Cu composite. J Mater Eng Perform 23:413–420. https://doi.org/10.1007/s11665-013-0768-8

20. Özdemir U, Sayer S, Yeni Ç (2012) Effect of pin penetration depth on the mechanical properties of friction stir spot welded aluminum and copper, Mater. TEST 54:233–239. https://doi.org/10.3139/120.110322

21. Zhang Z, Yang X, Zhang J, Zhou G, Xu X, Zou B (2011) Effect of welding parameters on microstructure and mechanical properties of friction stir spot welded 5052 aluminum alloy. Mater Des 32:4461–4470. https://doi.org/10.1016/j.matdes.2011.03.058

22. Kulekci MK (2014) Effects of process parameters on tensile shear strength of friction stir spot welded aluminium alloy (EN AW 5005). Arch Metall Mater 59:221–224. https://doi.org/10.2478/amm-2014-0035

23. Mubiayi MP, Titilayo Akinlabi E, Makhatha ME (2017) Microstructure and electrical resistivity properties of copper and aluminium friction stir spot welds. In 2017 8th International Conference on Mechanical and Intelligent Manufacturing Technologies (ICMIMT) 42–47. IEEE.

24. Saeid T, Abdollah-Zadeh AA, Sazgari B (2010) Weldability and mechanical properties of dissimilar aluminum–copper lap joints made by friction stir welding. J Alloy Compd 490(1–2):652–655

25. Colmenero AN, Orozco MS, Macías EJ, Fernández JB, Muro JCSD, Fals HC, Roca AS (2019) Optimization of friction stir spot welding process parameters for Al-Cu dissimilar joints using the energy of the vibration signals. Int J Adv Manuf Technol 100(9):2795–2802

26. Habibizadeh A, Honarpisheh M, Golabi SI (2021) Determining optimum shear strength of friction stir spot welding parameters of AA1050/C10100 joints. Manuf Technol 21(3):315–329

27. Jannet S, Mathews PK, Raja R (2015) Optimization of process parameters of friction stir welded AA 5083-O aluminum alloy using response surface methodology. Bull Polish Acad Sci Tech Sci 63:851–855. https://doi.org/10.1515/bpasts-2015-0097

28. Suryanarayanan R, Sridhar VG (2020) Effect of process parameters in pinless friction stir spot welding of Al 5754-Al 6061 alloys. Metallogr Microstruct Anal https://doi.org/10.1007/s13632-020-00626-5

29. Yuan W, Mishra RS, Webb S, Chen YL, Carlson B, Herling DR, Grant GJ (2011) Effect of tool design and process parameters on properties of Al alloy 6016 friction stir spot welds. J Mater Process Technol 211:972–977. https://doi.org/10.1016/j.jmatprotec.2010.12.014

30. Tozaki Y, Uematsu Y, Tokaji K (2008) Effect of tool shoulder diameter on mechanical properties of friction stir spot welded joints. Trans Japan Soc Mech Eng Part A 74:268–274. https://doi.org/10.1299/kikaia.74.268

31. Pandey AK, Mahapatra SS (2019) Investigation of weld zone obtained by friction stir spot welding (FSSW) of aluminium-6061 alloy. Mater Today Proc 18:4491–4500. https://doi.org/10.1016/j.matpr.2019.07.419

32. Karthikeyan R, Balasubramanian V (2010) Predictions of the optimized friction stir spot welding process parameters for joining AA2024 aluminum alloy using RSM. Int J Adv Manuf Technol 51:173–183. https://doi.org/10.1007/s00170-010-2618-2

33. Mishra RS, Ma ZY (2005) Friction stir welding and processing. Mater Sci Eng R Rep 50(1–2):1–78

34. Shen Z, Yang X, Zhang Z, Cui L, Yin Y (2013) Mechanical properties and failure mechanisms of friction stir spot welds of AA6061-T4 sheets. Mater Des 49:181–191

35. Bozkurt YAHYA, Salman S, Çam G (2013) Effect of welding parameters on lap shear tensile properties of dissimilar friction stir spot welded AA 5754–H22/2024-T3 joints. Sci Technol Weld Joining 18(4):337–345

36. Firouzdor V, Kou S (2012) Al-to-Cu friction stir lap welding. Metall Mater Trans A 43(1):303–315

37. Horie S, Shinozaki K, Yamamoto M, North TH (2010) Experimental investigation of material flow during friction stir spot welding. Sci Technol Weld Join 15, 666–670. [CrossRef]

38. Lin YC, Liu JJ, Chen JN (2013) Material flow tracking for various tool geometries during the friction stir spot welding process. J Mater Eng Perform 22, 3674–3683. [CrossRef]

39. Su P, Gerlich A, North TH, Bendzsak GJ (2006) Material flow during friction stir spot welding. Sci Technol Weld Joining 11(1):61–71

40. Balakrishnan M, Dinaharan I, Palanivel R, Sathiskumar R (2019) Effect of friction stir processing on microstructure and tensile behavior of AA6061/Al3Fe cast aluminum matrix composites. J Alloy Compd 785:531–541

41. Badarinarayan H, Yang Q, Zhu S (2009) Effect of tool geometry on static strength of friction stir spot-welded aluminum alloy. Int J Mach Tools Manuf 49(2):142–148